Central European Journal of Energetic Materials
ISSN 1733-7178; e-ISSN 2353-1843

Cent. Eur. J. Energ. Mater. 2020, *17*(1): 66-84; DOI 10.22211/cejem/118795
Article is available in PDF-format, in colour, at:
http://www.wydawnictwa.ipo.waw.pl/cejem/Vol-17-Number1-2020/CEJEM_01056.pdf

Research paper

Preparation and Characterization of CL-20 Based Composites by Compressed Air Spray Evaporation

Wen Zheng Xu*, Jin Yu Peng, Jie Wang, Hao Li, Jing Yu Wang

School of Environment and Safety Engineering, North University of China, 030051 Taiyuan, Shanxi, China
**E-mail: xuwznuc@126.com*

Abstract: Ultrafine CL-20 particles and three CL-20-based composites were prepared by a compressed air spray evaporation method. All samples were characterized by scanning electron microscopy (SEM), X-ray diffraction (XRD), differential scanning calorimetry (DSC) and mechanical sensitivity instruments. The results indicated that the thermal stabilities of the CL-20-based composites are better than that of ultrafine CL-20, and that the mechanical sensitivities of ultrafine CL-20 is lower than those of CL-20-based composites. The thermal stability and safety properties of CL-20/Estane 5703 are better than the other samples.

Keywords: CL-20, CL-20-based composites, thermal stability, mechanical sensitivity

1 Introduction

One of the main objectives of the development of high density energetic materials is to have higher energy and lower sensitivity [1]. Due to its superior performance, 2,4,6,8,10,12-hexanitro-2,4,6,8,10,12-hexaazaisoowurtzitane (CL-20) is regarded as the next generation of high-energy materials [2-4].

CL-20 has significantly greater energy and higher density than similar HMX-based compositions. Despite its outstanding energetic characteristics, the application range of CL-20 is still limited by its high mechanical sensitivity (impact sensitivity, friction sensitivity and static spark sensitivity *etc.*) and its easy crystal transformations [5, 6].

In recent years, reducing the mechanical sensitivity of CL-20 by different methods has aroused increasing academic interest. On the one hand, when the particle size of CL-20 is reduced, it becomes less sensitive and its decomposition rate decreases. Ultrafine CL-20 particles have lower sensitivity, high energy density, good stability and rapid energy release [7]. Hence, various methods have been reported for preparing energetic nanomaterials [8-13], such as grinding, milling, solvent-nonsolvent recrystallization, micro-emulsions, rapid expansion of supercritical solutions, sol-gel methods and vacuum co-deposition. On the other hand, formulations of conventional plastic bonded explosives can solve, to some extent, the problem of high sensitivity of CL-20. It should be noted that the surface coverage and mechanical strength are poor, and the morphology with large particles is inferior when the CL-20-based composites are prepared by the widely used water suspension method. These unfavorable factors may cause poor desensitization and structural instability in practical applications [14]. Therefore, how to combine these two aspects to prepare micro- or nanometer-sized composite particles is a difficult and meaningful problem. Fortunately, many researchers have shown that nanometer-sized spherical explosive particles, coated with a small amount of binder, can be prepared by a single-step, spray drying process [15-17].

Spray drying techniques are widely utilized to manufacture spherical nanosized particles. In recent years, many different types of inorganic nanoparticles [18, 19] have been prepared using spray drying. In the energetic materials field [20-22], the spray drying method is rarely used to manufacture nanosized explosives. In the present work, we prepared ultrafine CL-20 particles, and CL-20/Viton A, CL-20/AR-71 and CL-20/Estane 5703 composites by spray drying. Furthermore, the properties of these samples were characterized and analyzed in detail.

2 Experimental

2.1 Materials

Raw CL-20 was provided by Liaoning Qing Yang Special Chemicals Co., Ltd., China. Ethyl acetate (analytical reagent) was purchased

from Tianjin Tian da Chemicals Co., Ltd., China. AR-71 was purchased from the ZEON Company of United States. Viton A was purchased from Huizhou HaoYuan Plastic Raw Material Co., Ltd, China. Estane 5703 was purchased from Guang Dong Ming Ju Plastic Raw Material Co., Ltd, China.

2.2 Formation mechanism

The formation mechanisms of ultrafine CL-20 particles and the CL-20-based composite particles are similar. As shown in Figure 1, the formation of CL-20-based composites was by the compressed air spray evaporation method. Firstly, raw CL-20 and the binder were dissolved in ethyl acetate to form an homogeneous co-solution, and this co-solution was then transferred into a compressed air atomizing device. Compressed air through a small nozzle was used to form a high-speed jet which was streamed to generate a negative pressure to spray the mixed solution onto the fogging baffle. Due to the high-speed impact of the surrounding splash, the solution was transformed into droplets which were ejected from the spray outlet. These droplets were heated by the circulating heating device and caused the solvent to be evaporated. CL-20-based composites with a uniform and dense spherical form were formed.

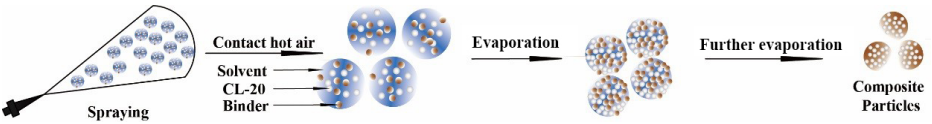

Figure 1. The formation mechanism of CL-20-based composites by compressed air spray evaporation

2.3 Preparation of ultrafine CL-20 particles and CL-20-based composites

The experimental device for preparing ultrafine CL-20 particles and the CL-20-based composites by compressed air spray evaporation is shown in Figure 2. The experimental procedure was as follows: both raw CL-20 (2.0000 g) and the binder (0.0408 g) were dissolved in ethyl acetate (20 cm^3) to form an homogeneous co-solution. The mass ratio of raw CL-20 to the binder was 98:2. As shown in Figure 2, the co-solution was poured into the atomization device. Meanwhile, the air compressor and the pressure control valve were opened to adjust the input air pressure of the compressor to 0.3 MPa. The droplets were then formed and sprayed from the atomization device at 1 cm^3/min. The droplets were sprayed into the drying tube and the solvent was rapidly evaporated. The temperature of the circulating heating device was 80 °C. Finally, the CL-20-based

composite particles were collected in the collection device after passing through the cyclone separator. The procedure for preparing ultrafine CL-20 particles was the same as for the preparation of the CL-20-based composite particles, the only difference being that a binder were not included when preparing ultrafine CL-20.

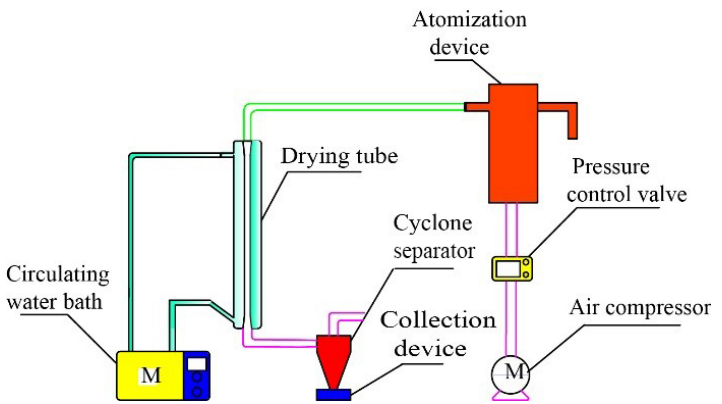

Figure 2. The experimental device for compressed air spray evaporation

2.4 Characterization

An SU8010 field-emission scanning electron microscope was used to characterize both the particle size and the morphologies of the ultrafine CL-20 particles and the CL-20-based composite particles. This equipment was manufactured by Hitachi Limited in Japan.

An X-ray diffractometer was used to identify the ultrafine CL-20 particles and the CL-20/binder composite particles. It was manufactured by China Dandong Hao Yuan Instrument Co., Ltd. The testing conditions included target material (Cu) with a tube voltage of 40 kV, a tube current of 30 mA, a 5° start angle and a 50° end angle.

The thermal decomposition characteristics of the samples were measured on a differential scanning calorimeter (DSC-131, France Setaram Corporation, Shanghai, China). The test conditions were as follows:

– nitrogen atmosphere: flow rate 30 cm^3/min,
– sample mass 0.7 mg,
– Al_2O_3 powder as reference material,
– the heating rates were 5, 10, 15, 20 °C/min.

The impact sensitivity was tested by a type 12 drop hammer apparatus according to GJB-772A-97 standard [23], method 601.3. The test conditions consisted of a drop weight of 2.500 ±0.002 kg, a sample mass of 35 ±1 mg,

at a relative humidity of 50%. A testing result was represented by a critical drop height of 50% explosion probability (H_{50}).

The friction sensitivity was tested with a WM-1 pendulum friction apparatus according to GJB-772A-97 standard [23], method 602.1. The test conditions consisted of a pendulum weight 1.5 kg; a swing angle of 66 ±1°; a pressure 2.45 ±0.07 MPa; sample mass 20 ±1 mg; and test number 25. The friction sensitivity is expressed as the explosion probability (P).

3 Results and Discussion

3.1 SEM characterization

Figure 3 shows the SEM morphologies of ultrafine CL-20 and the CL-20 based composites. As may be seen:

– the ultrafine CL-20 particles are a regular spherical shape without obvious defects on a smooth surface and with a narrow crystal size distribution of 200-300 nm (Figure 3(a)),
– the CL-20/Viton A composite particles are a regular spherical shape, and the particles are mainly distributed between 2 and 5 μm, and have a rough surface with holes (Figure 3(b)),
– the CL-20/AR-71 composite particles are a regular spherical shape, the particle size is uneven and dispersed, and there is slight agglomeration (Figure 3(c)),
– the CL-20/Estane 5703 composite particles are a regular spherical shape, and the particle size is concentrated in the range of 1-2 μm. The dispersion is better and the particles are dense (Figure 3(d)).

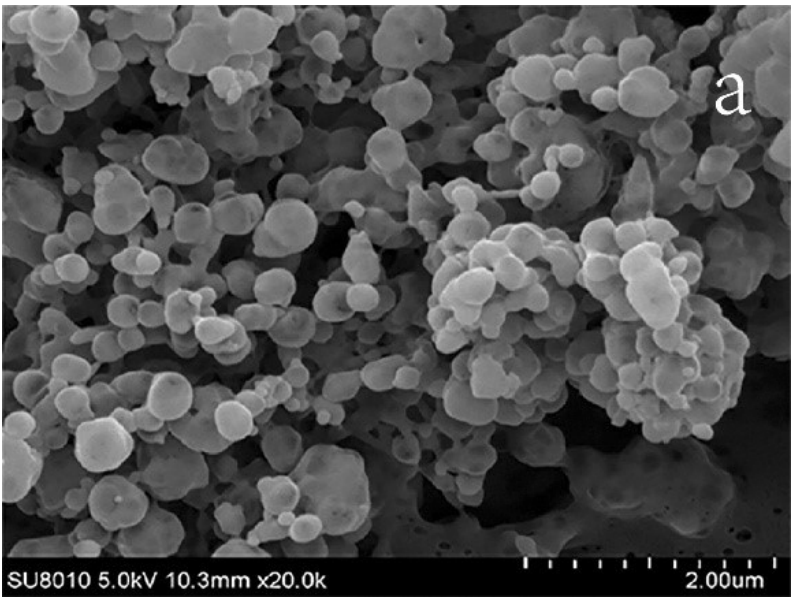

(a)

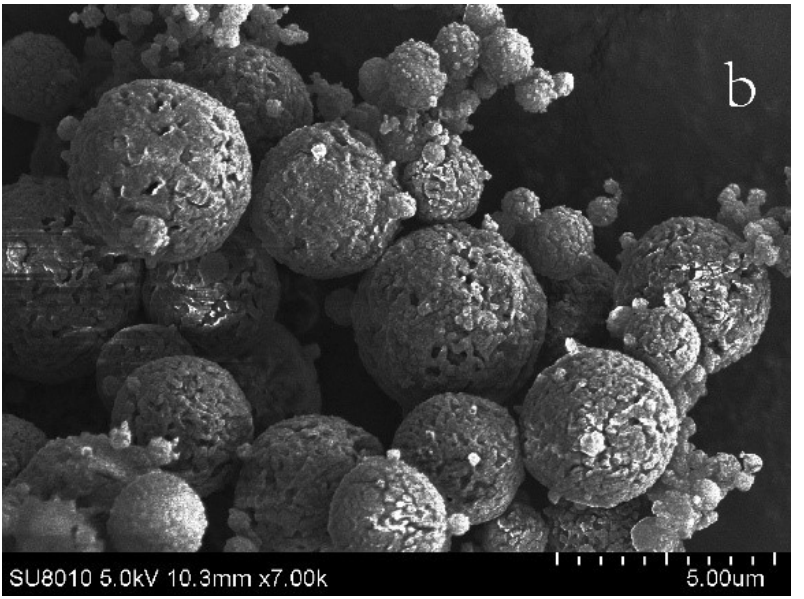

(b)

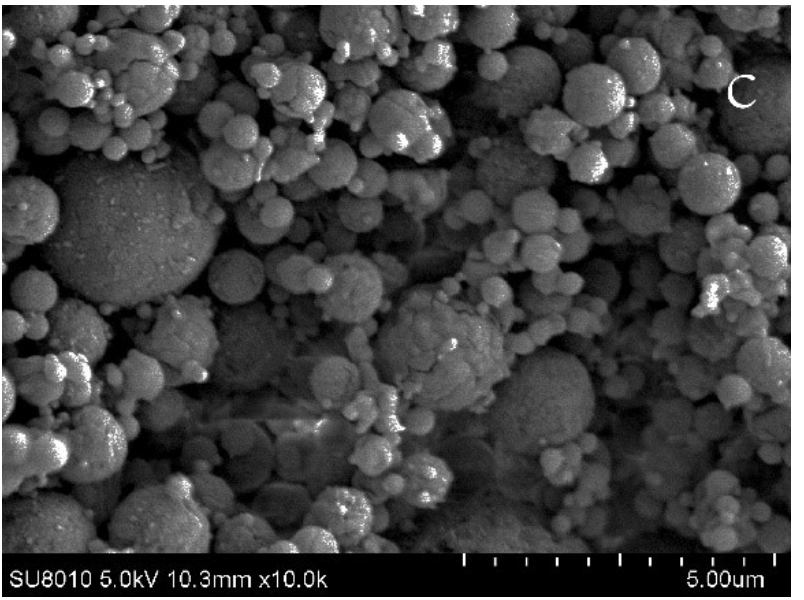

(c)

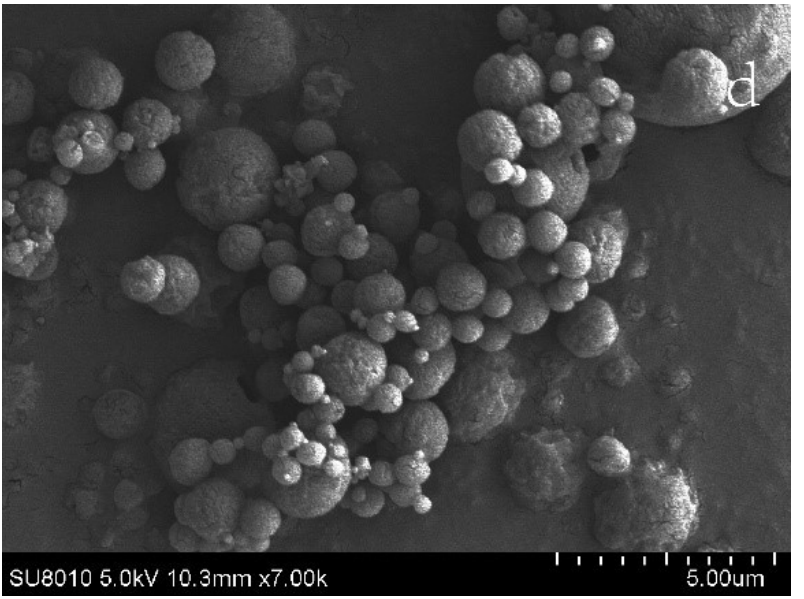

(d)

Figure 3. SEM images of (a) ultrafine CL-20 and (b-d) the CL-20-based composites (see text for identification)

3.2 XRD characterization

As temperature changes can cause phase changes in explosives [24-26], XRD was used to evaluate the ultrafine CL-20 and CL-20-based composites. The crystal structures of raw CL-20, ultrafine-CL-20 and the CL-20-based composites were investigated by their powder XRD patterns, which are shown in Figure 4. Raw CL-20 displayed three characteristic diffraction peaks at 12.6°, 13.8°, and 30.3°, which corresponds to the (11-1), (200), and (20-3) crystal faces 2Θ of the ε-phase (PDF Card 00-050-2045). Ultrafine-CL-20 and the CL-20 based composites exhibited different XRD patterns, and it was found that the patterns exhibited strong diffraction peaks at 13.6°, 24.1°, and 28.2°, which correspond to the (111), (212), and (132) crystal faces of the β-phase (PDF Card 00-052-2432). These results can be explained by Ostwald's rule [27] and solvent-mediated phase transitions (SMPT) [28, 29]. The recrystallization process of CL-20 involves a crystallizing process from solution. Thermodynamically, this tends to form the lowest free energy and most stable ε-crystal form; but in terms of kinetics, the formation and growth rates of metastable β-nuclei at the beginning are much faster than those of the ε-stabilized crystal form. So that the metastable crystal form is precipitated initially from solution. As the crystallization proceeds, ε-nucleation begins to grow, causing the concentration of the solution to decrease, and the metastable crystals to gradually dissolve, while the steady state crystals continue to grow. Finally, ε-CL-20 was obtained. But by the compressed air spray evaporation method, the solvent is evaporated rapidly, and the conditions for SMPT disappeared. Finally we obtained β-CL-20.

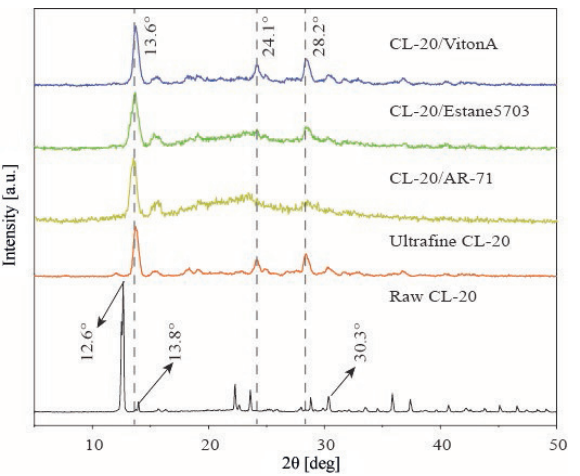

Figure 4. XRD patterns of raw CL-20, ultrafine CL-20 and the CL-20-based composites

3.3 Thermal decomposition characterization

Probing the kinetic and thermodynamic parameters is very important in mastering the thermolytic properties of energetic materials. Here, DSC traces of ultrafine CL-20 and the CL-20-based composites were obtained at different heating rates (Figure 5) and were used to calculate these parameters (Table 1). These DSC graphs show that the decomposition temperature and the heat output keep rising with increasing heating rate, from 5 to 20 °C/min. In addition, at the same heating rate, the exothermic peak temperatures of ultrafine CL-20 and the CL-20-based composites changes only slightly, indicating that the binder has no significant effect on the decomposition peak temperature of CL-20, and that the binders are compatible with CL-20.

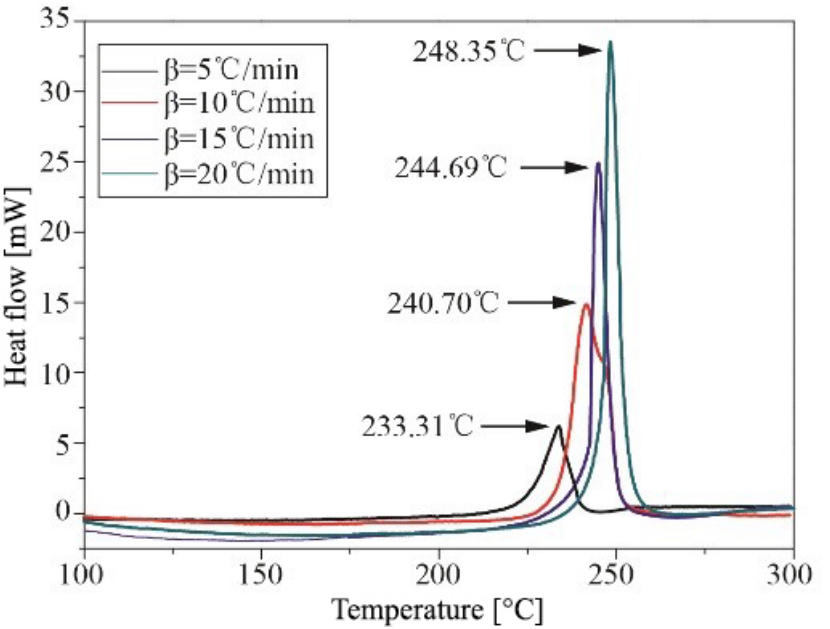

(a)

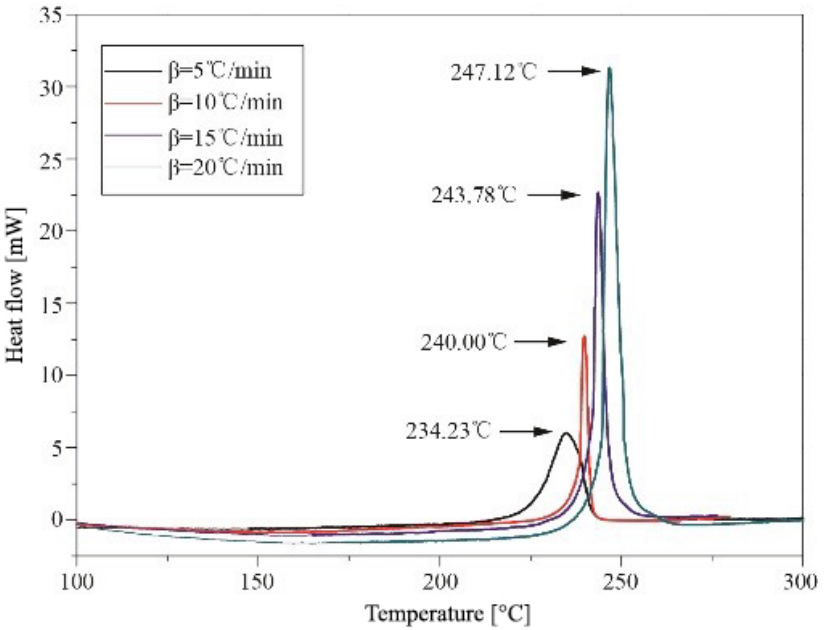

(b)

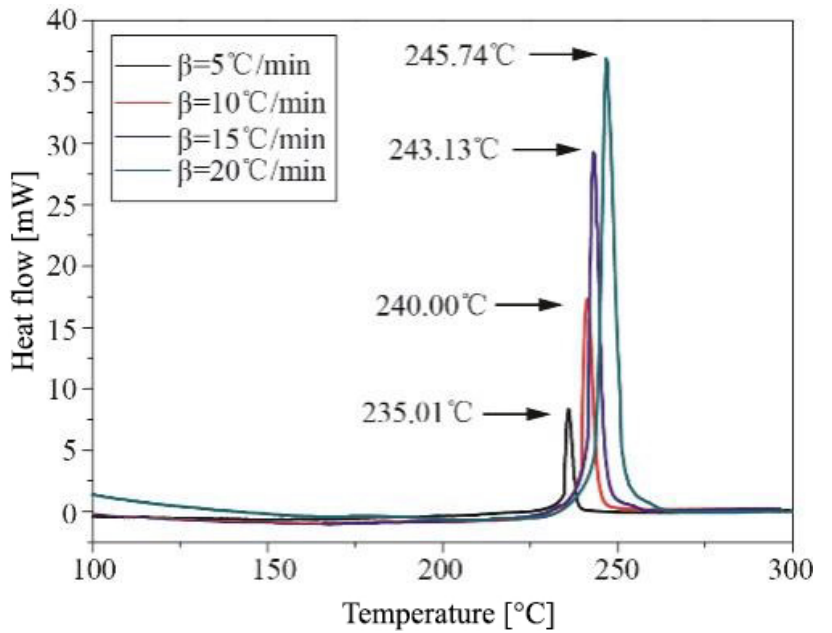

(c)

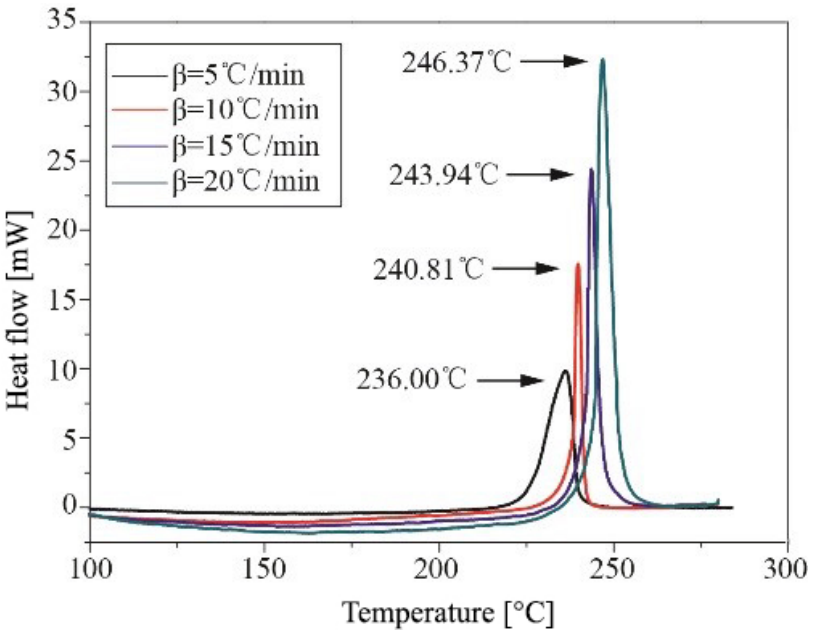

(d)

Figure 5. DSC curves of as-prepared samples collected at different heating rates for (a) ultrafine CL-20, (b) CL-20/Viton A, (c) CL-20/AR-71, (d) CL-20/Estane 5703

From the four exothermic peak temperatures at different heating rates, the Kissinger method [30] (Equation 1) and Rogers' method [31] (Equation 2) can be used to calculate the thermal decomposition kinetic parameters, activation energy (E_a) and pre-exponential factor (A), of ultrafine CL-20 and the CL-20-based composites.

$$\ln\left(\frac{\beta}{T_p^2}\right) = \ln\left(\frac{AR}{E_a}\right) - \frac{E_a}{RT_p} \tag{1}$$

$$A = \frac{E_a \beta}{RT_p^2} \exp\left(\frac{E_a}{RT_p}\right) \tag{2}$$

where T_p is the temperature of the exothermic peak in the DSC curve [K], β is the heating rate [K/min], E_a is the activation energy [J/mol], A is the pre-exponential factor, and R is the gas constant, 8.314 J/(mol·K).

From Table 1, the E_a values of CL-20/Viton A, CL-20/AR-71, and CL-20/Estane composites were 218.26, 243.10 and 252.45 kJ/mol, respectively. Compared to ultrafine-CL-20 (E_a = 186.42 kJ/mol), the E_a values of the CL-20-based composites were increased by 31.84, 56.68 and 66.03 kJ/mol, respectively. The plots of $\ln(\beta/T_p^2)$ against $1/T_p$ were straight lines for all samples (Figure 6). Figure 6 shows that the plots for the CL-20-based composites were close to that for ultrafine CL-20. This means that they undergo similar decomposition reactions.

Thermal stability is another important property of an explosive, which can be reflected in its shelf life. This can be expressed by its critical temperature of thermal explosion (T_b), which is defined as the lowest temperature at which a specific charge may be heated without undergoing thermal runaway [32]. In order to obtain the T_b values for these samples, Equations 3 and 4 were used [33, 34].

$$T_{pi} = T_{p0} + b\beta_i + c\beta_i^2 + d\beta_i^3 \qquad i = 1, 2, 3, 4 \tag{3}$$

$$T_b = \frac{E_a - \sqrt{E_a^2 - 4RE_aT_{p0}}}{2R} \tag{4}$$

where T_{p0} is the extrapolated onset temperature at the heating rate closest to 0 K; and T_b is the critical explosion temperature [K]. The T_{p0} and T_b were calculated and are listed in Table 1.

Table 1. Thermal explosion and critical temperature data for ultrafine CL-20 and the CL-20-based composites

Samples	Kinetics		Thermal stability		Thermodynamic data	
	E_a [kJ/mol]	ln$A$	T_{p0} [K]	T_b [K]	$\Delta G^{\neq}$ [kJ/mol]	$\Delta H^{\neq}$ [kJ/mol]
Ultrafine CL-20	186.42	37.93	492.60	503.93	153.76	182.32
CL-20/Viton A	218.26	45.65	498.07	505.90	153.34	214.12
CL-20/Estane 5703	252.45	58.69	501.68	509.60	132.72	248.29
CL-20/AR-71	243.10	56.53	499.97	508.13	132.73	238.94

As is illustrated in Table 1, the T_b of ultrafine CL-20, and the CL-20/Viton A, CL-20/AR-71 and CL-20/Estane 5703 composites were 503.93, 505.90, 508.13, and 509.60 K, respectively. Compared with ultrafine CL-20, it was easily found that the T_b values of the CL-20-based composites were increased

by 1.97, 4.20 and 5.67 K. This shows that the critical explosion temperature of the CL-20-based composites is practically higher than that of ultrafine CL-20.

The decomposition of ultrafine CL-20 and the CL-20-based composites complies with the decomposition mechanism of monomolecular energetic materials. That is to say, the molecule originates from the activation and rupture of its weakest bond. This course dominates the entire decomposition process and can be depicted by the parameters of activation enthalpy ($\Delta H^{\neq}$) and activation free energy ($\Delta G^{\neq}$), which are calculated by Equations 5 and 6 [35].

$$\mathrm{A}\exp\frac{-E_a}{RT}=\frac{k_BT}{h}\exp\frac{-\Delta G^{\neq}}{RT} \tag{5}$$

$$\Delta \mathrm{H}^{\neq}=\mathrm{E}_a-RT_{p0} \tag{6}$$

where k_B and h are the Boltzmann ($k_B = 1.381\cdot10^{-23}$ J/K) and Planck constants ($h = 6.626\cdot10^{-34}$ J/s), respectively. $\Delta H^{\neq}$ is the energy that the molecules must absorb to change from the common state to the activated state; thus, the value of $\Delta H^{\neq}$ was much closer to that of E_a for each sample. Comparing the data in Table 1, we found that ultrafine CL-20 need the lowest energy for activation, *i.e.* ultrafine CL-20 is the easiest to be activated. CL-20/Estane 5703 needs the highest energy for activation. $\Delta G^{\neq}$ is the chemical potential of the activation course. For all samples, the values of $\Delta G^{\neq}$ were positive numbers. This means that none of the activation processes proceeded spontaneously. In summary, the thermal stabilities of the CL-20-based composites are therefore slightly better than that of ultrafine CL-20. CL-20/Estane 5703 has the best thermal stability.

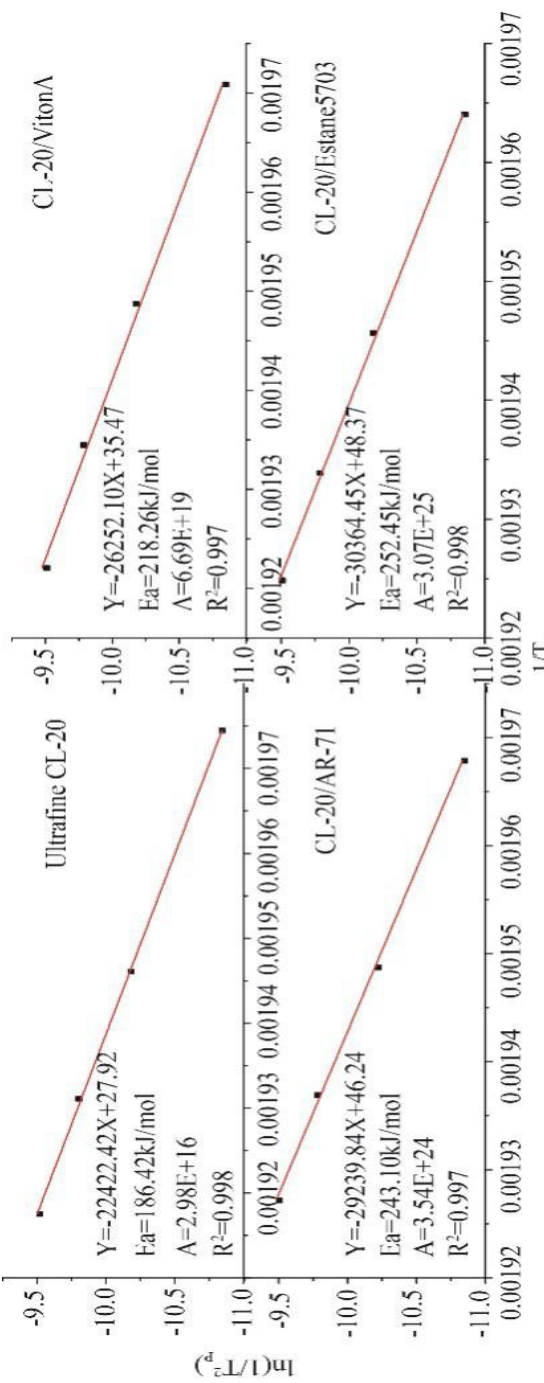

Figure 6. Kissinger plots of ultrafine CL-20, CL-20-based composites

3.4 Mechanical sensitivity characterization

Mechanical sensitivity is a challenge in an explosive's detonation under mechanical actions, such as impact and friction. Under normal circumstances, the special height (H_{50}) of impact and the explosion probability (P) of friction reflect the sensitivity of an explosive, the higher the H_{50} or the lower the P, the less sensitive the explosive, and thus higher safety. As shown in Figure 7(a), the H_{50} of ultrafine CL-20 was 21.5 cm. The H_{50} values of CL-20/Viton A, CL-20/AR-71 and CL-20/Estane 5703 were increased by 6.16, 11.12 and 14.30 cm, respectively. For the friction sensitivity, the P value of ultrafine CL-20 was 96%; the P values of CL-20/Viton A, CL-20/AR-71 and CL-20/Estane 5703 changed from 96% to 96%, 88%, and 84% (Figure 7(b)), respectively. The mechanical sensitivities of the CL-20-based composites were reduced significantly. At the same time, we found that Estane 5703 is superior to Viton A and AR-71 in reducing the mechanical sensitivity of CL-20.

In theory, when the tiny pores and voids are subjected to adiabatic compression, there would be a very fast elevation of the temperature inside the pores. When the temperature exceeded the critical temperature, hot spots would be formed [36]. Hot spots can cause thermal decomposition or even explosion of explosives. Therefore, the mechanical sensitivity test results can be explained well by the critical explosion temperature. The lower the critical explosion temperature, the easier it is for hot spots to form and the lower the safety of the explosive.

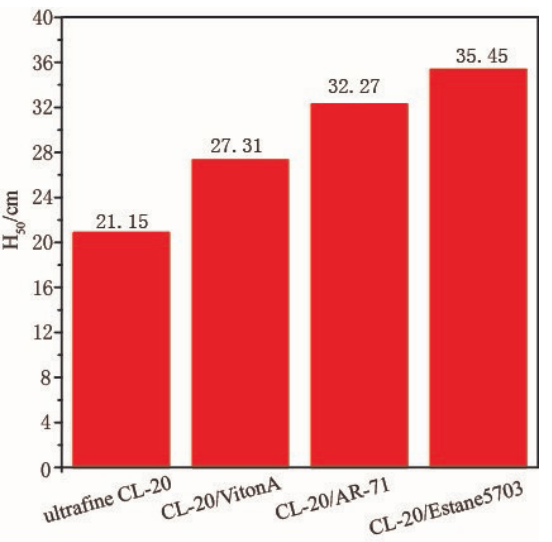

(a)

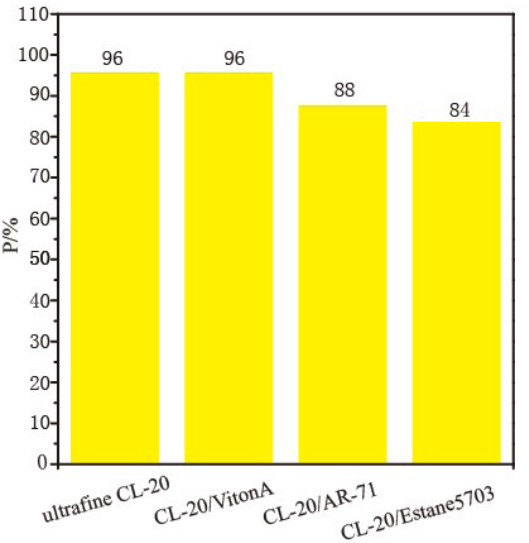

(b)

Figure 7. (a) Impact- and (b) friction sensitivities of the explosive samples

4 Conclusions

Ultrafine CL-20 and CL-20-based composites were successfully prepared by the compressed air spray evaporation method. The thermal stability of the CL-20-based composites was found to be better than that of ultrafine CL-20, and the mechanical sensitivity of ultrafine CL-20 was higher than that of the CL-20-based composites. Compared with ultrafine CL-20, these CL-20-based composites have better thermal stability and safety. In addition, the sample of CL-20/Estane 5703 exhibited excellent thermal stability and safety properties. Estane 5703 is thus very suitable as the binder in CL-20-based plastic bonded explosives.

References

[1] Sivabalan, R.; Gore, G.M.; Nair, U.R.; Saikia, A.; Venugopalan, S.; Gandhe, B.R. Study on Ultrasound Assisted Precipitation of CL-20 and Its Effect on Morphology and Sensitivity. *J. Hazard. Mater.* **2007**, *139*(2): 199-203.

[2] Nair, U.R.; Sivabalan, R.; Gore, G.M.; Geetha, M.; Asthana, S.N.; Singh, H.

Hexanitrohexaazaisowurtzitane (CL-20) and CL-20-based Formulations (Review). *Combust. Explos. Shock Waves* **2005**, *41*(2): 121-132.

[3] Geetha, M.; Nair, U.R.; Sarwade, D.B.; Gore, G.M.; Asthana, S.N.; Singh, H. Studies on CL-20: the Most Powerful High Energy Material. *J. Therm. Anal. Calorim.* **2003**, *73*(3): 913-922.

[4] Nielsen, A.T.; Christian, S.L.; Moore, D.W. Synthesis of 3,5,12-Triazawurtzitane (3,5,12-triazatetracyclo[5.3.1.1^{2,6}0^{4,9}]dodecanes). *J. Therm. Anal. Calorim.* **1987**, *52*(9): 1656-1662.

[5] Urbelis, J.H.; Swift, J.A. Solvent Effects on the Growth Morphology and Phase Purity of CL-20. *Cryst. Growth Des.* **2014**, *14*(4): 1642-1649.

[6] Mandal, A.K.; Thanigaivelan, U.; Pandey, R.K.; Asthana, S.; Khomane, R.B.; Kulkarni, B.D. Preparation of Spherical Particles of 1,1-Diamino-2,2-dinitroethene (FOX-7) Using a Micellar Nanoreactor. *Org. Process Res. Dev.* **2012**, *16*(11): 1711-1716.

[7] Gupta, S.; Kumar, P.D.; Sharma, S.; Kaur, G.; Agarwal, A.; Lata, P. Pressurized Nozzle-based Solvent/Anti-solvent Process for Making Ultrafine ε-CL-20 Explosive. *Propellants Explos. Pyrotech.* **2017**, *42*(7): 773-783.

[8] Gao, H.; Liu, J.; Hao, G.Z.; Xiao, L.; Qiao, Y. Study on Preparation, Characterization and Comminution Mechanism of Nano-sized CL-20. *Chin. J. Explos. Propellants* **2015**, *2*(38): 46-49.

[9] Bayat, Y.; Zeynali, V. Preparation and Characterization of Nano-CL-20 Explosive. *J. Energ. Mater.* **2011**, *29*: 281-291.

[10] Bayat, Y.; Zarandi, M.; Zarei, M.A.; Soleyman, R.; Zeynali, V. A Novel Approach for Preparation of CL-20 Nanoparticles by Microemulsion Method. *J. Mol. Liq.* **2014**, *193*: 83-86.

[11] Krause, H.; Löbbecke, S.; Marioth, E.; Teipel, U.; Thome, V. Screening Units for Particle Formation of Explosives using Supercritical Fluids. *Int. Annu. Conf. Fraunhofer ICT,* **2000**, *31*: 119.

[12] Wang, Y.; Song, X.L.; Song, D.; Jiang, W.; Liu, H.Y.; Li, F.S. A Versatile Methodology Using Sol-Gel, Supercritical Extraction, and Etching to Fabricate a Nitramine Explosive: Nanometer HNIW. *J. Energ. Mater.* **2013**, *31*(1): 49-59.

[13] Pivkina, A.; Ulyanova, P.; Frolov, Y.; Zavyalov, S.; Schoonman, J. Nanomaterials for Heterogeneous Combustion. *Propellants Explos. Pyrotech.* **2004**, *29*(1): 39-48.

[14] Ye, B.Y.; An, C.W.; Wang, J.Y.; Geng, X.H. Formation and Properties of HMX-based Microspheres *via* Spray Drying. *RSC Adv*. **2017**, *7*(56): 35411-35416.

[15] Zhigach, A.N.; Leipunskii, I.O.; Berezkina, N.G; Pshechenkov, P.A.; Zotova, E.S.; Kudrov, B.V.; Gogulya, M.F.; Brazhnikov, M.A.; Kuskov, M.L. Aluminized Nitramine-based Nanocomposites: Manufacturing Technique and Structure Study. *Combust. Explos. Shock Waves* **2009**, *45*(6): 666-677.

[16] Qiu, H.; Stepanov, V.; Stasio, A.R.D.; Chou, T.; Lee, W.Y. RDX-based Nanocomposite Microparticles for Significantly Reduced Shock Sensitivity. *J. Hazard. Mater.* **2011**, *185*(1): 489-493.

[17] An, C.W.; Li, H.Q.; Geng, X.H.; Li, J.L.; Wang, J.Y. Preparation and Properties

of 2,6-Diamino-3,5-dinitropyrazine-1-oxide based Nanocomposites. *Propellants Explos. Pyrotech.* **2013**, *38*(2): 172-175.
[18] Suh, W.H.; Suslick, K.S. Magnetic and Porous Nanospheres from Ultrasonic Spray Pyrolysis. *J. Am. Chem.* Soc. **2005**, *127*(34): 12007-12010.
[19] Bang, J.H.; Suslick, K.S. Applications of Ultrasound to the Synthesis of Nanostructured Materials. *Adv. Mater.* **2010**, *22*(10): 1039-1059.
[20] Kim, J.W.; Shin, M.S.; Kim, J.K.; Kim, H.S.; Koo, K.K. Evaporation Crystallization of RDX by Ultrasonic Spray. *Ind. Eng. Chem. Res.* **2011**, *50*(21): 12186-12193.
[21] Spitzer, D.; Risse, B.; Schnell, F.; Pichot, V.; Klaumunzer, M.; Schaefer, M.R. Continuous Engineering of Nano-cocrystals for Medical and Energetic Applications. *Sci. Rep.* **2014**, *4*: 6575.
[22] Risse, B.; Spitzer, D.; Hassler, D.; Schnell, F.; Comet, M.; Pichot, V.; Muhr, H. Continuous Formation of Submicron Energetic Particles by the Flash-evaporation Technique. *Chem. Eng. J.* **2012**, *203*: 158-165.
[23] *Explosive Test Method.* Chinese National Military Standard GJB/772A-97, **1997**.
[24] Smilowitz, L.; Henson, B.; Asay, B.; Dickson, P. A Model of the *β*-δ Phase Transition in PBX9501. *Shock Compression Condens. Matter* **2001**, 1077-1080.
[25] Saw, C.K. Kinetics of HMX and Phase Transitions: Effects of Grain Size at Elevated Temperature. *Int. Det. Symp.*, *Proc., 12th*, San Diego, **2002**.
[26] Gump, J.C.; Peiris, S.M. Phase Transitions and Isothermal Equations of State of *epsilon* Hexanitrohexaazaisowurtzitane (CL-20). *J. Appl. Phys.* **2008**, *104*(8): 1.
[27] Threlfall, T. Structural and Thermodynamic Explanations of Ostwald's Rule. *Org. Process Res. Dev.* **2003**, *7*(6): 1017-1027.
[28] Mangin, D.; Puel, F.; Veesler, S. Polymorphism in Processes of Crystallization in Solution: A Practical Review. *Org. Process Res. Dev.* **2009**, *13*(1): 1-32.
[29] Croker, D.; Hodnett, B.K. Mechanistic Features of Polymorphic Transformations: The Role of Surfaces. *Cryst. Growth Des.* **2010**, *10*(6): 2806-2816.
[30] Kissinger, H.E. Reaction Kinetics in Differential Thermal Analysis. *Anal. Chem.* **1957**, *29*(11): 1702-1706.
[31] Rogers, R.N.; Dauh, G.W. Scanning Calorimetric Determination of Vapor-phase Kinetics Data. *Anal. Chem.* **2002**, *45*(3): 596-600.
[32] Burnham, A.K.; Weese, R.K.; Wemhoff, A.P.; Maienschein, J.L. A Historical and Current Perspective on Predicting Thermal Cookoff Behavior. *J. Therm. Anal. Calorim.* **2007**, *89*(2): 407-415.
[33] Zhang, T.L.; Hu, R.Z.; Xie, Y.; Li, F.P. The Estimation of Critical Temperatures of Thermal Explosion for Energetic Materials using Non-isothermal DSC. *Thermochim. Acta.* **1994**, *244*: 171-176.
[34] Sovizi, M.R.; Hajimirsadeghi, S.S.; Naderizadeh, B. Effect of Particle Size on Thermal Decomposition of Nitrocellulose. *J. Hazard. Mater.* **2009**, *168*(2-3): 1134-1139.
[35] Wang, Y.; Song, X.L.; Song, D.; Li, L.; An, C.W.; Wang, J.Y. Synthesis, Thermolysis, and Sensitivities of HMX/NC Energetic Nanocomposites. *J. Hazard. Mater.* **2016**, *312*: 73-83.

[36] Wang, S.; An, C.W.; Wang, J.Y.; Ye, B.Y. Reduce the Sensitivity of CL-20 by Improving Thermal Conductivity Through Carbon Nanomaterials. *Nanoscale Res. Lett.* **2018**, *13*(1): 85.

Received: April 1, 2019
Revised: March 16, 2020
First published online: March 20, 2020